Few-Cycle Light Bullets Created by Femtosecond Filaments

L. Bergé* and S. Skupin

Département de Physique Théorique et Appliquée, CEA-DAM/Ile de France, B.P. 12, 91680 Bruyères-le-Châtel, France

(Received 27 September 2007; published 18 March 2008)

We report a generic mechanism of light bullet formation during the filamentation of femtosecond pulses. This mechanism is tested for gaseous and dense media. It allows the production of robust, sub-10 fs structures of light with no post-compression stage. By coupling an infrared pump with a seed beam, tunable pulses with durations down to a few femtoseconds can be generated by parametric processes.

DOI: 10.1103/PhysRevLett.100.113902 PACS numbers: 42.65.Tg, 42.68.Ay, 52.38.Hb

Self-guided filaments created from ultrashort laser pulses are exploited in various areas of physics, from atmospheric remote sensing to high harmonic generation (see, e.g., [1] for review). Their basic physics relies on the Kerr-induced self-focusing process, which makes the laser intensity increase up to the ionization threshold. Once ionization occurs, the resulting electron plasma defocuses the pulse, which then propagates like a narrow channel of light. Recently, emphasis has been put on the possibility to shorten the pulse through this mechanism, by letting nonlinearities confine its temporal profile into a single peak of a few femtoseconds in pressurized cells of noble gas [2–5]. Most experiments using this principle succeeded in achieving pulse shortening down to 4–5 fs after, however, a post-compression stage. In parallel, Théberge *et al.* [6] recently exploited four-wave mixing (4WM) inside the filament to produce pulsed beams with excellent quality at tunable wavelengths. Tested in argon as well as in air, the resulting 4WM pulses could attain about 10-fs durations after passing across a prism compressor.

Propagation regimes allowing pure self-compression actually need to be identified for, e.g., optimizing high-order harmonic signals [7]. Despite the previous studies, no analysis has been performed for characterizing structures of light able to reach durations of few optical cycles over long ranges, while keeping a flat phase. The present work demonstrates the genericity of such few-cycle ''light bullets'' through the filamentation process. By investigating femtosecond filaments close to their saturation threshold, we display evidence that light bullets with sub-10 fs durations can be created in various materials. Furthermore, we propose to combine both techniques of self-compression by filamentation and tunability via 4WM for creating light pulses of 5 fs, generated at visible wavelengths without a post-compression technique. We evaluate the length scales upon which temporal compression becomes optimal versus spectral distortions. Numerical simulations reveal the intimate mechanism by which 4WM pulses can be compressed by filamentation. Finally, we analyze the spectral broadening around the third harmonic, yielding pulses with durations ≤ 3 fs in the corresponding spectral window. Direct diagnostics for identifying these light bullets are proposed.

Our propagation model governs the unidirectional spectral amplitude of the laser field as [1,8–10]

$$\partial_z \hat{E} = \frac{i}{2k(\omega)} \nabla_\perp^2 \hat{E} + ik(\omega)\hat{E} + \frac{i\mu_0 \omega^2}{2k(\omega)} \hat{\mathcal{F}}_{\mathrm{NL}}, \qquad (1)$$

where $\hat{E}(r, z, \omega)$ is the Fourier transform of the forward electric field component, z is the propagation variable, $\nabla_\perp^2 = r^{-1}\partial_r r \partial_r$ is the diffraction operator, $k(\omega) = n(\omega)\omega/c$ is the wave number of the optical field for a medium with refractive index $n(\omega)$ at frequency ω. $\hat{\mathcal{F}}_{\mathrm{NL}} \equiv \hat{P}_{\mathrm{NL}} + i\hat{J}/\omega$ is the Fourier transform of the nonlinearities that include the nonlinear polarization P_{NL}, the current density J created by charged particles and related plasma losses. We consider a cubic susceptibility tensor $\chi^{(3)}$ constant in frequency [11], so that $P_{\mathrm{NL}} = \epsilon_0 \chi^{(3)} E^3$. For pulse propagation in atom gases, stimulated Raman scattering is ignored. For propagation in silica, the cubic nonlinearity is delayed in ratio 0.15 by Raman scattering [12]. When free electrons are created, the current density $J = q_e \rho v_e$ evolves with the electron charge q_e, velocity v_e, and density $\rho(r, z, t)$, which is described by

$$\partial_t \rho = W(I)(\rho_{\mathrm{nt}} - \rho) + \frac{\sigma}{U_i}\rho I - \frac{\rho}{\tau_r}. \qquad (2)$$

Here, I is the field intensity and Eq. (1) is completed by ionization losses defined by $J_{\mathrm{loss}} E = U_i W(I)(\rho_{\mathrm{nt}} - \rho)$. Plasma sources include photoionization processes with the rate $W(I)$ derived by Perelomov, Popov, and Terent'ev for gases [13] or by Keldysh for solids [14]; ρ_{nt} and U_i are density of neutral species and ionization potential. Collisional ionization has the cross section σ and τ_r is the time for electron recombination, taken as infinite in argon and equal to 150 fs in silica. The full propagation model (1) will be employed for treating third-harmonic generation produced by the cubic nonlinearity $\sim E^3$ at the end of the present work. Before that discussion, light bullets and 4WM will be described from the standard envelope model inferred from (1) when one fixes a central pump frequency associated with an envelope function U such that $E \sim U e^{ik(\omega_0)z - i\omega_0 t}$ + c.c. In this case, the Kerr response $\sim n_2 |U|^2 U$ with index n_2 contains the nonlinearities necessary for 4WM. Both unidirectional and envelope

models, together with parameter values for argon and silica, can be found recalled in Ref. [1]. We checked that the envelope model provides spectra similar to those computed from the spectral equation (1) in the frequency range $\omega \leq 5 \times 10^{15}$ Hz that excludes third-harmonic generation (THG) at 800 nm. Propagation equations are integrated for either one pump component or from the superposition of input fields $U(z=0) = \sum_{j=0,s} A_j e^{-i(\omega_j - \omega_0)t}$, where the indices $j = 0, s$ refer to the pump and seed pulses, respectively. A_j denotes Gaussian envelope distributions,

$$A_j(r, z=0, t) = \sqrt{\frac{2P_{\rm in}^j}{\pi w_j^2}} e^{-(r^2/w_j^2)-(t^2/t_j^2)}, \qquad (3)$$

with partial powers $P_{\rm in}^j$, waist w_j, and $1/e^2$ time extent t_j. Partial energies $E_{\rm in}^j \equiv \sqrt{\pi/2} t_j P_{\rm in}^j$ satisfy $E_{\rm in}^s \ll E_{\rm in}^0$.

To start with, we simulate a single pulse at 800 nm in a 1 m long cell of argon with pressure $p = 0.5$ atm. Experimental setups with appropriate focusing geometries currently produce narrow beams with waist $w_0 \sim 150$ μm near focus and short durations, e.g., $t_0 = 25$ fs. We thus examine the fate of ultrashort pulses from the filamentation onset using these parameters. With an input power equal to critical ($P_{\rm in} = P_{\rm cr} \simeq \lambda_0^2/2\pi n_0 n_2$), the pulse slightly increases in intensity up to its peak value $I_{\rm max} \simeq 75$ TW/cm^2 with maximal plasma level $\rho_{\rm max} \simeq 8 \times 10^{15}$ cm^{-3}, during the first 20 cm of propagation [Fig. 1(a)]. The evolution pattern in the (t, z) plane [Fig. 1(b)] reveals that at farther distances it reaches shorter and shorter durations, as the plasma slowly turns off. The temporal profile remains singly peaked, with about 8 fs FWHM duration kept over more than 20 cm after $z \simeq 0.5$ m. This relaxation stage after plasma defocusing refers to what we henceforth call the "light bullet" regime, along which the pulse propagates with an almost constant intensity $I_b > 10$ TW/cm^2 and small duration $t_b \leq 10$ fs. A similar mechanism drives the self-compression of filaments reported in Ref. [15]. We can observe a slight deflection of the pulse towards positive times, which is caused by steepening effects. Inspection of the numerical data reveals the net tendency of the pulse to decrease its power slightly below critical, in order to reach a quasistable state with no further self-focusing. Although weak, the plasma response remains important in this regime. It not only prevents wave collapse, but also assures a smooth waveguiding at low electron densities $<10^{14}$ cm^{-3} and prevents pulse splitting in time.

Few-cycle light bullets can also be created in dense materials, such as fused silica. Figures 1(c)–1(e) report the evolution of Gaussian pulses at the three wavelengths $\lambda_0 = 800$, 1275, and 1550 nm, with respective coefficients for group-velocity dispersion of 370, -1.93, and -280 fs^2/cm. The input power is increased to 1.2 $P_{\rm cr}$, in order to overcome reduction of the effective Kerr index by the Raman response. The pulse develops one focusing-defocusing sequence. Again, maximal compression is observed as the pulse starts to diffract. Typical minimal durations are 13 fs at 800 nm, 9 fs at 1275 nm, and 8 fs at 1550 nm. Negative group-velocity dispersion drives extended collapse events and shrinks more the pulse duration over longer distances [16–18]. Compared with gases, however, the asymptotic stage of self-compression is small, because dense materials favor strong dispersion and rapid spreading.

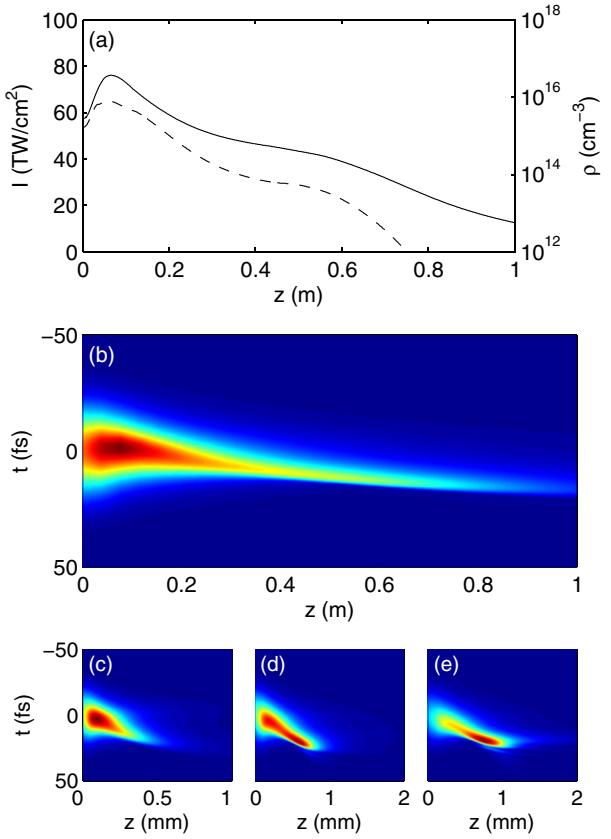

FIG. 1 (color online). (a) Peak intensity (solid line, left axis) and peak electron density (dashed line, right axis) of a 150 μm-waisted, 25 fs Gaussian pulse propagating in argon at critical power for $\lambda_0 = 800$ nm and $p = 0.5$ atm. (b) On-axis temporal profiles versus propagation distance. (c)–(e) Same for 800 nm, 25 fs Gaussian pulses with 1.2 critical power in silica at (c) $\lambda_0 = 800$ nm, $w_0 = 4$ μm, (d) $\lambda_0 = 1275$ nm, $w_0 = 7$ μm, and (e) $\lambda_0 = 1550$ nm, $w_0 = 9.6$ μm.

Next, we examine the copropagation of the pulse shown in Fig. 1(b) with a 13 μJ seed pulse ($E_{\rm in}^s = E_{\rm in}^0/50$) having the input characteristics $t_s = 50$ fs, $w_s = w_0$ at $\lambda_s = 1500$ nm. Following Ref. [6], we couple a near-infrared filament at 800 nm (central frequency ω_0) with a low-intensity seed pulse at a larger wavelength (ω_s), for generating components at a visible frequency $\omega_{\rm 4WM} = 2\omega_0 - \omega_s$ ($\lambda_{\rm 4WM} = 550$ nm). Figure 2(a) shows that this wave coupling preserves a light bullet regime in argon. Peak values of the overall intensity and plasma density remain close to those attained in Fig. 1(a). The pulse, once satu-

rated, produces a long-living waveform keeping a short duration along 50 cm. Note the periodicity of the most intense optical distributions, which corresponds to interferences at $\omega_0 - \omega_s$ between pump and seed. In Fig. 2(b)–2(d), we show the on-axis spectrum of the entire pulse at different propagation distances. Along the plasma stage, the spectrum contains discrete peaks broadened by self- and cross-phase modulations, which can be identified for all components, namely, from left to right: the seed, pump, 4WM frequency and related cascaded process ($2\omega_{4WM} - \omega_0$). At short distances $z \simeq 10$ cm, the 4WM component gains energy along distances that remain of the order of the conversion length L_{4WM}. This length is evaluated from the linear phase mismatch parameter $\Delta k_{4WM} = k(2\omega_0 - \omega_s) - 2k_0 + k_s \simeq 0.12\ \mathrm{cm}^{-1}$ and from the nonlinearities. Applying plane wave estimates [19], the optical index is affected by the interplay of nonlinearities, $\Delta n_{NL} = n_2 I - \rho(I)/2n_0\rho_c$, and this modifies the coherence length as

$$L_{4WM} \simeq \frac{\pi}{\Delta k_{4WM} + 2\frac{\omega_0}{c}\Delta n_{NL}}. \quad (4)$$

Inserting the peak values of Fig. 1(a) and the critical density $\rho_c = 1.73 \times 10^{21}\ \mathrm{cm}^{-3}$, we readily find $L_{4WM} \approx 9$ cm along which the 4WM frequency builds up, which is confirmed numerically [Fig. 2(b)]. Upon longer scales, down-conversion takes place and both the seed and 4WM pulse amplitudes decrease [Fig. 2(c)]. Beyond a few coherence lengths, the supercontinuum generation of the pump develops sharply towards the blue wavelengths and overlaps the discrete spectral components. The distance at which this process occurs is evaluated from the onset of optical shocks induced by self-steepening that produces a large blueshift, i.e., $L_{cr} \simeq \sqrt{e/2}t_b c/(3n_2 I_b)$ [20]. Assuming a Gaussian shape for the light bullet, we find $L_{cr} \simeq 0.4$ m during its early propagation ($t_b \sim 10$ fs, $I_b \sim 60\ \mathrm{TW/cm}^2$ after 0.2 m). This evaluation agrees with the spectral distortions shown in Fig. 2(d).

To diagnose light bullets, it is worth exploiting their decrease in intensity and plasma density to levels which may be inspected *in situ* as the pulse attains the shortest durations ($\rho \leq 10^{14}\ \mathrm{cm}^{-3}$ from $z \geq 0.35$ m). In terms of spectral signatures, light bullets can also be experimentally identified through their cross correlation frequency-resolved optical gating (XFROG) traces [15]. Figures 2(e) and 2(f) illustrate computed XFROG traces in the bandwidth centered around the pump [2(e)] and 4WM [2(f)] frequencies. FWHM pulse durations corresponding to these spectral domains are 9 and 4 fs, respectively. All frequency components are aligned at the same delay time, indicating a flat spectral phase. This property should be preserved when the pulse exits through thin enough ($\ll 1$ mm) glass windows. To compensate for dis-

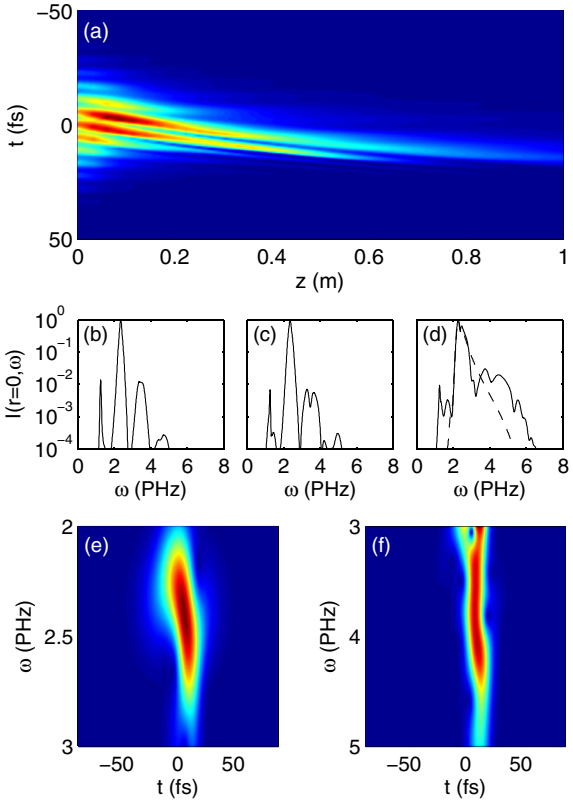

FIG. 2 (color online). (a) Same as Fig. 1(b), but with a copropagating ~13 μJ, 50 fs seed pulse at 1500 nm. Corresponding spectra at (b) $z = 0.1$ m, (c) $z = 0.15$ m, and (d) $z = 0.5$ m. The dashed line in (d) shows the spectrum without the seed pulse (see Fig. 1). XFROG traces of (e) the pump pulse and (f) the 4WM pulse at $z = 0.35$ m. Different color scales were used to improve visibility in (f).

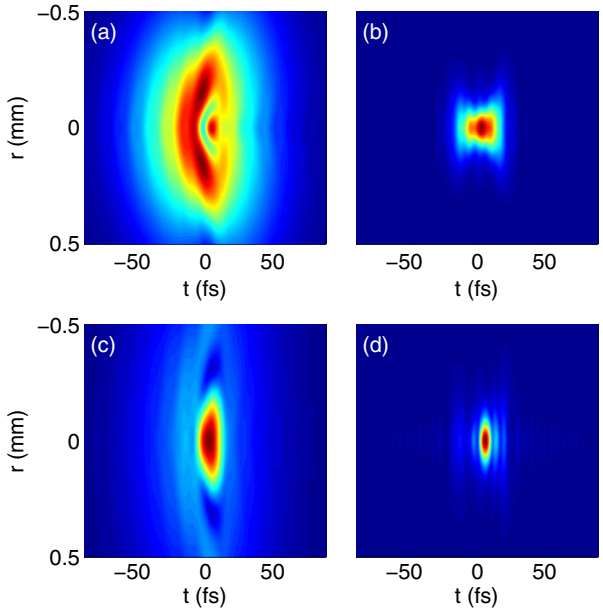

FIG. 3 (color online). Intensity distribution of (a) seed and (b) 4WM pulses at $z = 0.15$ m. The spectral filter is (a) $\lambda >$ 1040 nm and (b) $450 < \lambda < 650$ nm, respectively. (c),(d) Same at the distance $z = 0.25$ m. Energy in the 4WM spectral region (d) is ~6 μJ; FWHM pulse duration is 5.5 fs.

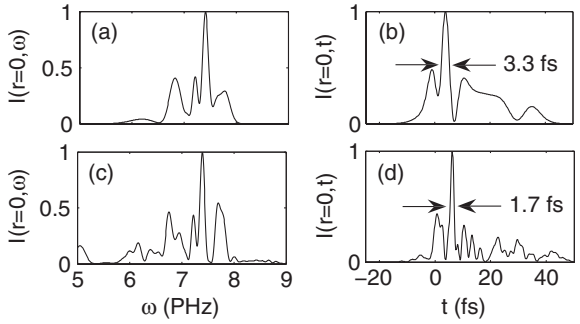

FIG. 4. On-axis spectra and normalized temporal profiles for THG in the wavelength window $210 < \lambda < 375$ nm: (a),(b) without the seed pulse at $z = 0.2$ m and (c),(d) with the seed at $z = 0.25$ m. Shortest FWHM durations are pointed out.

persive spreading by thicker windows, negative dispersion can be introduced into the beam path [3].

Figure 3 details the dynamical behavior of the seed and 4WM pulses, computed from the total field after applying appropriate spectral filters. Needing two photons at frequency ω_0, these pulses both augment in intensity over 10 cm, until they reach values of $I_s \simeq 0.4$ TW/cm^2 and $I_{4\mathrm{WM}} \simeq 3$ TW/cm^2. At $z = 0.15$ m, the seed and 4WM pulses undergo down-conversion [Figs. 3(a) and 3(b)]. The inner part of the seed pulse is depleted before raising again near center. At $z = 0.25$ m, both components regain energy and focus at center, in such a way that the 4WM pulse becomes compressed to a few femtoseconds only [Figs. 3(c) and 3(d)]. Energy exchanges cease afterwards and the 4WM pulse saturates around $I_{4\mathrm{WM}} \simeq 6$ TW/cm^2 within the intensity ratio $I_{4\mathrm{WM}}/I_s \sim 10$. Four-wave mixing pulse durations as short as 4–5 fs are attained and they are preserved up to 0.5 m in the light bullet regime. The energy contained in the generated pulse is about 6 μJ, which corresponds to 46% of the initial seed energy. This result is consistent with the conversion efficiency measurements reported in Ref. [6]. The generated pulses are issued from the parametric couplings of the pump and seed envelopes through the cubic nonlinearities $\sim 2|A_0|^2 A_{4\mathrm{WM}} + A_0^2 A_s^* e^{-i\Delta k_{4\mathrm{WM}} z}$ [19], which trap light in waveforms with effective durations less than that of the carrier filament.

Finally, we also investigated the spectral zone of THG ($\lambda_{\mathrm{TH}} \simeq 266$ nm). Analysis was performed using the full unidirectional model (1) which allows generation of high-order frequencies. In the absence of seed, the frequency window above 5×10^{15} Hz reveals the early emergence of third-harmonic (TH) at $z = 0.05$ m, which then broadens along z. This produces pulses developing ultrashort spikes whose effective FWHM duration can locally reach 3.3 fs [Figs. 4(a) and 4(b)]. Parametric sources varying like E^3 create TH pulses whose duration is at least equal to the pump duration divided by $\sqrt{3}$. It can decrease more due to the broadening of the TH bandwidth. In the presence of a seed, more satellite frequencies are generated by cascading in this spectral interval. The resulting spectrum is thus larger and favors even sub-2 fs pulses [Figs. 4(c) and 4(d)]. It must be noticed that these subpulses were found less stable than the pump and 4WM components, as they could not hold their temporal shape over long propagation ranges.

In conclusion, we have numerically demonstrated the existence of generic light bullets compressed to the few-cycle limit in filamentation regime with no external compressor system. These can be formed in gaseous as well as dense media. By coupling the pump with a lower-amplitude seed pulse, optical components generated by four-wave mixing can be emitted at visible wavelengths and propagate over long distances with a stable profile shrunk to 5 fs durations. TH pulses with even shorter durations can naturally be produced, but they were found to be less robust along the optical path.

*luc.berge@cea.fr

[1] L. Bergé, S. Skupin, R. Nuter, J. Kasparian, and J. P. Wolf, Rep. Prog. Phys. **70**, 1633 (2007).
[2] S. Champeaux and L. Bergé, Phys. Rev. E **68**, 066603 (2003).
[3] C. P. Hauri, W. Kornelis, F. W. Helbing, A. Heinrich, A. Couairon, A. Mysyrowicz, J. Biegert, and U. Keller, Appl. Phys. B **79**, 673 (2004).
[4] A. Couairon, M. Franco, A. Mysyrowicz, J. Biegert, and U. Keller, Opt. Lett. **30**, 2657 (2005).
[5] G. Stibenz, N. Zhavoronkov, and G. Steinmeyer, Opt. Lett. **31**, 274 (2006).
[6] F. Théberge, N. Aközbek, W. Liu, A. Becker, and S. L. Chin, Phys. Rev. Lett. **97**, 023904 (2006).
[7] H. S. Chakraborty, M. B. Gaarde, and A. Couairon, Opt. Lett. **31**, 3662 (2006).
[8] A. V. Husakou and J. Herrmann, Phys. Rev. Lett. **87**, 203901 (2001).
[9] M. Kolesik, J. V. Moloney, and M. Mlejnek, Phys. Rev. Lett. **89**, 283902 (2002).
[10] J. Liu, H. Schroeder, S. L. Chin, R. Li, W. Yu, and Z. Xu, Phys. Rev. A **72**, 053817 (2005).
[11] C. G. Durfee III, S. Backus, H. C. Kapteyn, and M. M. Murnane, Opt. Lett. **24**, 697 (1999).
[12] A. A. Zozulya, S. A. Diddams, A. G. Van Engen, and T. S. Clement, Phys. Rev. Lett. **82**, 1430 (1999).
[13] A. M. Perelomov, V. S. Popov, and M. V. Terent'ev, Sov. Phys. JETP **24**, 207 (1967).
[14] L. V. Keldysh, Sov. Phys. JETP **20**, 1307 (1965).
[15] S. Skupin, G. Stibenz, L. Bergé, F. Lederer, T. Sokollik, M. Schnürer, N. Zhavoronkov, and G. Steinmeyer, Phys. Rev. E **74**, 056604 (2006).
[16] L. Bergé and S. Skupin, Phys. Rev. E **71**, 065601(R) (2005).
[17] K. D. Moll and A. L. Gaeta, Opt. Lett. **29**, 995 (2004).
[18] J. Liu, R. Li, and Z. Xu, Phys. Rev. A **74**, 043801 (2006).
[19] G. P. Agrawal, *Nonlinear Fiber Optics* (Academic, San Diego, 2001), 3rd ed.
[20] D. Anderson and M. Lisak, Phys. Rev. A **27**, 1393 (1983).